ORIGINAL ARTICLE

JBMR®

The Development of Dentin Microstructure Is Controlled by the Type of Adjacent Epithelium

Josef Lavicky,[1] Magdalena Kolouskova,[1] David Prochazka,[2] Vladislav Rakultsev,[1] Marcos Gonzalez-Lopez,[1] Klara Steklikova,[3,4] Martin Bartos,[5,6] Anushree Vijaykumar,[7] Jozef Kaiser,[2] Pavel Pořízka,[2] Maria Hovorakova,[3] Mina Mina,[7] and Jan Krivanek[1]

[1]Department of Histology and Embryology, Faculty of Medicine, Masaryk University, Brno, Czech Republic
[2]Advanced Instrumentation and Methods for Materials Characterization, CEITEC Brno University of Technology, Brno, Czech Republic
[3]Institute of Histology and Embryology, First Faculty of Medicine, Charles University, Prague, Czech Republic
[4]Department of Cell Biology, Faculty of Science, Charles University, Prague, Czech Republic
[5]Institute of Dental Medicine, First Faculty of Medicine, Charles University, Prague, Czech Republic
[6]Institute of Anatomy, First Faculty of Medicine, Charles University, Prague, Czech Republic
[7]Department of Craniofacial Sciences School of Dental Medicine, University of Connecticut, Farmington, CT, USA

ABSTRACT

Considerable amount of research has been focused on dentin mineralization, odontoblast differentiation, and their application in dental tissue engineering. However, very little is known about the differential role of functionally and spatially distinct types of dental epithelium during odontoblast development. Here we show morphological and functional differences in dentin located in the crown and roots of mouse molar and analogous parts of continuously growing incisors. Using a reporter (DSPP-cerulean/DMP1-cherry) mouse strain and mice with ectopic enamel (Spry2$^{+/-}$;Spry4$^{-/-}$), we show that the different microstructure of dentin is initiated in the very beginning of dentin matrix production and is maintained throughout the whole duration of dentin growth. This phenomenon is regulated by the different inductive role of the adjacent epithelium. Thus, based on the type of interacting epithelium, we introduce more generalized terms for two distinct types of dentins: cementum versus enamel-facing dentin. In the odontoblasts, which produce enamel-facing dentin, we identified uniquely expressed genes (*Dkk1*, *Wisp1*, and *Sall1*) that were either absent or downregulated in odontoblasts, which form cementum-facing dentin. This suggests the potential role of Wnt signalling on the dentin structure patterning. Finally, we show the distribution of calcium and magnesium composition in the two developmentally different types of dentins by utilizing spatial element composition analysis (LIBS). Therefore, variations in dentin inner structure and element composition are the outcome of different developmental history initiated from the very beginning of tooth development. Taken together, our results elucidate the different effects of dental epithelium, during crown and root formation on adjacent odontoblasts and the possible role of Wnt signalling which together results in formation of dentin of different quality. © 2021 The Authors. *Journal of Bone and Mineral Research* published by Wiley Periodicals LLC on behalf of American Society for Bone and Mineral Research (ASBMR).

KEY WORDS: TEETH; DENTIN; MICROSTRUCTURE; ODONTOBLAST; PROCESSES; ODONTOGENESIS; DENTINOGENESIS; INCISOR; MOLAR; WNT SIGNALING; LIBS

Introduction

Teeth are highly specialized structures with an intricate inner architecture, positioned at the very beginning of the digestive system. They are important for food processing and essential for social interactions not only in humans but in other species as well. Apart from the soft dental pulp, which is responsible for the maintenance of tooth viability, teeth are composed of three different types of calcified tissues: enamel, dentin, and cementum. The general shape, mechanical properties, and functions of teeth are determined by dentin, the most abundant and ontogenetically first developing hard dental tissue. Enamel, as the hardest

Received in original form June 5, 2021; revised form October 12, 2021; accepted November 8, 2021.
Address correspondence to: Jan Krivanek, PhD, Department of Histology and Embryology, Faculty of Medicine, Masaryk University, Brno, Czech Republic. E-mail: jan.krivanek@med.muni.cz
Additional Supporting Information may be found in the online version of this article.
JL and MK contributed equally to this work.
Journal of Bone and Mineral Research, Vol. 37, No. 2, February 2022, pp 323–339.
DOI: 10.1002/jbmr.4471

and the most calcified dental tissue, protects the most exposed part of the tooth — the crown. Cementum covers the root surface and, together with periodontal ligaments, maintains the anchoring of teeth in the adjacent alveolar bone. Dentin, in contrast to enamel, is a living tissue, which, alongside pulp, forms dentin-pulp complex.[1] This integrated functional unit maintains tooth homeostasis and enables the tooth to react to the outer environment.[2-6]

Odontoblasts are responsible for dentin development and maintenance of its viability and sensitivity. They are polarized, long-living cells positioned on the interface between the dental pulp and dentin itself.[7] Odontoblasts differentiate from ectomesenchyme after an orchestrated interaction with oral epithelium.[8,9] During tooth development, two basic types of oral epithelium can be distinguished: the enamel-forming epithelium and the epithelium, which plays a role in the development of the root. Enamel-forming oral epithelium in the crown gives rise to enamel-producing ameloblasts, while oral epithelium in the root forms Hertwig's epithelial root sheath (HERS), which does not produce any hard matrix and serves as an interactive partner for differentiating odontoblasts. After initiation of dentin production, HERS disintegrates into epithelial cell rests of Malassez (ERM).[8,10-13] This means that odontoblasts forming the crown and root dentin have a different interactive epithelial partner. The influence of oral epithelium on the determination of the different character of the adjacent dentin's microstructure and elemental composition has not yet been studied.

As odontoblasts lay down the dentin matrix, they are pushed back from the dental epithelium toward the dental pulp and leave behind a single, long process, which then persists inside the dentin matrix.[14] Odontoblasts' processes (also known as Tomes' fibers) are the key structural and functional components of dentin and make this tissue sensitive and able to react to the outer environment. This is particularly important in the process of tertiary dentinogenesis, a process that can be referred to as dental healing.[15,16] Odontoblasts contribute to sensing and reacting to increased tooth wear or dental caries by thickening the dental wall and thus prolonging the life span of teeth.[15] Interestingly, although dentin is a living tissue (similar to bone), once dentin is formed, it is not remodelled as it occurs in bone; therefore, dentin inner structure is determined during its formation.[17]

On the molecular level, the dentin matrix is formed by the calcification of the protein network, which is synthesized by the odontoblasts. This protein network is predominantly composed of collagen I fibrils but also several other non-collagenous proteins. Among the most abundant non-collagenous proteins belongs dentin sialophosphoprotein (DSPP) and dentin matrix acidic phosphoprotein 1 (DMP1), which serve as key mineralization centers.[8] Through the expression and phosphorylation of these proteins, odontoblasts regulate the rate of dentin matrix calcification.[18,19] Both proteins are highly expressed by odontoblasts.[20] Although, in contrast to DMP1, which is also expressed by other hard tissue–forming cells (osteoblasts/−cytes, cementoblasts/−cytes),[21,22] DSPP is specifically expressed within odontoblasts, which makes DSPP a unique molecular marker suitable for odontoblast detection and characterization. In this work, we focus on the differences between the microstructure of dentin in the crown (labial aspect of incisor) and the root (lingual aspect of incisor). Because we used genetically altered organisms, which have an ectopic enamel on the lingual aspect of mouse incisors, we are introducing more generalized terms: cementum-facing dentin and enamel-facing dentin.

Here we show, using different genetically altered animals and various methodological approaches, an unanticipated site-dependent microstructure of dentin in high detail. Our results show that the lingual and labial aspects of mouse incisors fully reflect the crown and root aspect in brachyodont teeth in the perspective of the microstructure of dentin and also the presence of cementum-forming cells in the periodontium. Further, we show a different gene expression pattern in odontoblasts on the labial and lingual aspect as well as the elemental composition and X-ray density in each type of dentin. Finally, using a mouse strain with ectopic enamel on the lingual aspect of the incisor, we confirm that the microstructure of dentin is dependent on the interaction with a different type of adjacent epithelium during development. Taken together, we hypothesize that the dentin microstructure is initially induced by the type of adjacent dental epithelium present during the beginning of odontoblast differentiation and influenced by Wnt signalling.

Materials and Methods

Animals

Animals used in this study included *DSPP*^{Cerulean}/*DMP1*^{Cherry} reporter mouse strain on CD-1 genetic background,[23] *Spry2*$^{+/-}$;*Spry4*$^{-/-}$ mice[24,25] obtained by crossing the strains Spry2/ORF-null allele and Spry4/ORF-null allele (originally a kind gift from Dr Ophir Klein, San Francisco, UCSF[26,27]) on C57BL/6 genetic background, and C57BL/6 wild-type animals, which were used as controls. All animal experiments were approved by the Ministry of Education, Youth and Sports, Czech Republic (MSMT-8360/2019–2; MSMT-9231/2020–2; MSMT-272/2020–3) and performed according to international and local regulations. All mice were kept in a 12-hour light/dark cycle, 18°C to 23°C and 40% to 60% humidity. Animals had access to food and water *ad libitum*. Animals were genotyped using endpoint PCR utilizing transgene/mutation-specific primers. Both male and female mice were used. Adult (2-month-old) animals with suitable genotype were euthanized by isoflurane overdose (KDG9623, Baxter, Deerfield, IL, USA) and cervical dislocation and further utilized for experiments.

Histological analysis

Mandibles and maxillae were carefully dissected, briefly washed in PBS, and fixed in 4% paraformaldehyde (pH 7.4) for 5 hours at 4°C. Fixed tissue was then decalcified in 10% EDTA (pH 7.4) for 10 days at 4°C. Samples were then processed either for cryosectioning or paraffin processing. Briefly, for cryosectioning, samples were incubated in 30% sucrose (Sigma-Aldrich, St. Louis, MO, USA; 16104) overnight at 4°C, washed twice in Tissue-Tek OCT Compound (Sakura Finetek Europe B.V., Alphen aan den Rijn, Netherlands; 4583) and embedded in fresh OCT. Samples used to obtain detail images were then sectioned to a thickness of 14 μm on cryostat Leica CM1860 (Leica Biosystems, Wetzlar, Germany). To obtain overview images of the mandible and maxilla of *DSPP*^{Cerulean}/*DMP1*^{Cherry}, samples were sectioned to a thickness of 40 μm using Kawamoto's tape (SECTION-LAB Co. Ltd., Hiroshima, Japan) on cryostat Leica CM1860 (Leica Biosystems). Samples embedded in paraffin were sectioned on a microtome (Leica SM2000R) to a thickness of 2 μm and processed as described further.

In situ hybridization

For the in situ hybridization, RNAscope 2.5 HD Assay – RED (Advanced Cell Diagnostics, Newark, CA, USA; 322350) was utilized as described before.[28] The following probes were used: Dkk1 (501921) and Wisp1 (402521). Slides were counterstained with hematoxylin for 1 minute and mounted in Pertex medium (Histolab, Brea, CA, USA; 00801). Sections were imaged using Axio Imager 2 (Carl Zeiss AG, Jena, Germany).

Immunostaining, confocal imaging, and image analysis

All cryosections were washed three times in PBS with 0.1% Tween 20 (Sigma-Aldrich, P1379). Sections from *DSPP*^{Cerulean}/*DMP1*^{Cherry} animals were stained with DAPI (Carl Roth, Karlsruhe, Germany; 6335.1) and mounted in VECTASHIELD Antifade mounting medium (Vector Laboratories, Burlingame, CA, USA; H-1000-10). Sections from wild-type and *Spry2*$^{+/-}$;*Spry4*$^{-/-}$ animals were stained with Phalloidin-Alexa Fluor 488 (Cell Signaling Technology, Danvers, MA, USA; 8878S) diluted 1:100 in PBS (pH 7.4) overnight at 4°C. Sections were then subsequently stained with DAPI and mounted in 87.5% Glycerol (Penta CZ, Katovice, Czech Republic) diluted in PBS. For the detection of periostin (POSTN), sections from *DSPP*^{Cerulean}/*DMP1*^{Cherry} animals were stained with anti-POSTN antibody (Novus Biologicals, Littleton, CO, USA; NBP1-30042) diluted 1:200 overnight at 4°C. Subsequently, the sections were stained with donkey anti-rabbit secondary antibody conjugated with Alexa Fluor 647 (Thermo Fisher Scientific, Waltham, MA, USA; A31573) diluted 1:500 at room temperature for 2 hours. Sections were then stained with DAPI and mounted using VECTASHIELD Antifade mounting medium. For the analysis of the expression of odontoblast-specific markers, SALL1 antibody (Abcam, Cambridge, MA, USA; ab31526) and NFIC antibody (Novus, NBP2-37935) were used. SALL1 staining was performed on paraffin sections after pH 9 antigen retrieval (Agilent Dako, Santa Clara, CA, USA; S2367) at 95°C for 15 minutes. NFIC staining was performed on cryosections from wild-type animals without antigen retrieval. Sections were incubated with antibodies overnight at 4°C. Subsequently, donkey anti-rabbit secondary antibody conjugated with Alexa Fluor 568 (Thermo Fisher Scientific, A10042) diluted 1:800 was used, and nuclei were counterstained with DAPI (Carl Roth, 6335.1). Slides were then mounted in Fluoromount Aqueous Mounting Medium (Sigma-Aldrich, F4680). Sections were imaged using LSM880 confocal microscope (Carl Zeiss AG, Germany). Obtained data were then analyzed and exported using Imaris (Oxford Instruments, Abingdon, UK) and ZEN software (Carl Zeiss AG, Germany).

Process straightness analysis

Segmentation was performed in Imaris using semiautomatic approach. Each of the randomly selected odontoblast processes (OPs) were traced using a single polyline. Dendrite straightness parameter was chosen for the quantification. This parameter is defined as the ratio between the length of the whole segmented polyline (OP) and the radial distance between the beginning and the end of the polyline. The value of the function is always equal to or smaller than 1 (a completely straight line has the straightness of 1). We compared 10 randomly chosen processes per each condition.

Process width analysis

For the analysis of odontoblast process width, confocal images of the phalloidin-stained sagittal sections were used. Images were analyzed using Imaris software. The width of the processes was measured using the measure distance tool in the slice mode. The measurement was performed at the beginning of dentin (above the predentin) at the unified distance of 40 μm from the dentin-pulp edge. For each experimental condition, 85 individual processes were measured.

Process number density analysis

The number density of processes was analyzed using coronal sections of dentin and from Z projections of sagittal sections of dentin obtained in the section mode of Imaris software. Subsequently, the processes were manually counted using ImageJ software, utilizing the point tool. The number of processes was counted on four unique regions of interest. All of the regions of interest used for the analysis contained at least 75 unique processes.

Analysis of dentin fraction without the presence of the main process

The distance from the furthermost point of processes main filament up to the enamel-dentin or cementum-dentin junction (= height of dentin without the presence of the main process) and total height of dentin in the corresponding place was measured using the measure distance tool in the slice mode of Imaris software. To obtain the fraction of dentin without the presence of the main process, the height of dentin without main OP was divided by the total dentin height. A total of 33 unique processes per experimental condition were analyzed.

Analysis of the distribution of processes in dentin

The unified 10-μm-thick Z-stacks were created using ZEN Blue software's (Carl Zeiss AG) employing the image subset function. Z-stacks were exported as maximum-intensity projections using Imaris software. Subsequently, the images were analyzed in ImageJ software.[29] Binary single-channel images were produced using the threshold function. A 10×10 grid was overlayed over the image using the grid overlay plugin. Using the rectangle selection tool and the overlayed grid, 10 equal sectors (parallel with the dentin-pulp edge) were analyzed using the measure function. The area fraction parameter was then used for the final analysis. The analysis was performed on three images per experimental condition.

Analysis of the distance from cervical loop to the first reporter expression

Sagittal sections containing the cervical loop region of incisors from maxillae and mandibles of the *DSPP*^{Cerulean}/*DMP1*^{Cherry} animals were analyzed. The distance from the apex of the cervical loops to the first odontoblast displaying either cerulean, cherry, or both signals above the background level was measured using the measure polyline tool in the slice mode in the Imaris software. The distance was measured both on the labial and lingual sides of the incisors. A total of eight sections (four animals, two sections each) were analyzed.

Calcified matrix analysis

For the analysis of the elemental composition of the incisor and micro-CT analysis, wild-type Bl/6 animals were overdosed by isoflurane (KDG9623, Baxter), the mandibles and maxillae were then carefully dissected, briefly washed in PBS, and fixed in 4% paraformaldehyde (pH 7.4) overnight at 4°C. Fixed tissues were then dehydrated in ethanol (30%, 50%, 70%, 80%, 90%, 96%, 100%) in each solution three times for 10 minutes and subsequently embedded into epoxy adhesive LR White (Sigma-Aldrich, L9774). The blocks containing the embedded mandibles and maxillae were cut using a diamond saw and sections were polished using abrasive papers P1500 and P3000.

Laser-induced breakdown spectroscopy (LIBS) analysis

The polished samples were placed in the interaction chamber, which is a part of the LIBS Discovery device (CEITEC BUT, Brno, Czech Republic). As the laser source Nd:YAG laser CFR-400 (Quantel, Lannion, France; 20 Hz, 532 nm, 10 ns) was employed. The laser pulse energy was controlled by a motorized attenuator (Eksma Optics, Vilnius, Lithuania) and was kept constant (30 mJ/pulse) throughout the experiment. The laser beam was focused on the sample surface with a glass triplet (Sill optics, DE, f = 32 mm). The resulting spot size diameter was 30 μm. Plasma radiation was collected using two UV-grade lenses with a total focal length of 75 mm and led via optical cable (400 μm, Thorlabs, Newton, NJ, USA) to the entrance of a spectrometer (HR2000, Ocean Optics, Orlando, FL, USA). The precise timing of the experiment was controlled by the digital pulse generator (SyncRay, Lightigo, Brno, Czech Republic). The gate delay was set to 1.5 μs and gate width to 50 μs. All measurements were controlled by a computer equipped with LIBS control software (Lightigo). The spatial resolution for all measurements was determined by the laser spot size diameter and was set at 30 μm in both directions. Obtained data were processed using the R software (R Foundation for Statistical Computing, Vienna, Austria).

Micro-CT evaluation of dentin structure

Selected specimens (sectioned teeth in PMMA block) were scanned using desktop micro-CT SkyScan 1272 (Bruker microCT, Kontich, Belgium). Specimens were fixed on specimen holder and scanned under the following scanning parameters: 0.5 μm pixel size, source voltage 60 kV, source current 166 μA, 0.25 mm Al filter, rotation step of 0.1°, frame averaging = 2, 180° rotation, scanning time ~9 hours for each specimen. The flat-field correction was updated before each acquisition. Projection images were reconstructed into cross-section images using NRecon software (Bruker). 2D visualizations were achieved using DataViewer (Bruker).

The X-ray density of dentin was analyzed using ImageJ software. Briefly, five square, regularly distributed selections per enamel, enamel- and cementum-facing dentins, were analyzed using the measure function. Mean grey value was then used for the final analysis. A total of 25 selections per tissue type were analyzed (five images, five selections per tissue type each).

Statistical analysis

Data were analyzed using Graph Pad Prism software (GraphPad Software, La Jolla, CA, USA). First, the normality of the data was assessed using Anderson-Darling (A2*), D'Agostino-Pearson omnibus (K2), Shapiro–Wilk (W), Kolmogorov–Smirnov (distance) tests, and QQ plots. If the data passed normality tests and *F* test to determine whether they have equal variances, a two-tailed *t*-test was used for the analysis. If the data did not pass normality tests, a two-tailed Mann–Whitney test was used to analyze the data. Subsequently, box plots and violin plots were constructed to visualize the obtained data. Box plots were made to display the interquartile range (25th to 75th percentile). Whiskers were used to indicate upper and lower extremes (1.5 × interquartile range). Outliers were shown in red. When the number of data was less than 20, all points were shown. To visualize the data obtained from the analysis of the distribution of processes in dentin, the trend was traced through the medians of the respective regions with whiskers showing the whole range of values. The trends were tested using Pearson's linear correlation of medians from the individual data sets. This analysis was performed in MATLAB (MathWorks, Natick, MA, USA) programming language using a built-in linear of rank correlation (corr) function (testing a null hypothesis of no correlation against the alternative hypothesis of a nonzero correlation). The critical *p*-value for statistical significance was set to $p = 0.05$.

Results

The microstructure of odontoblasts' processes in the crown and roots of molars is reflected by the labial and lingual aspects of incisors

To investigate the microstructure of OPs in different parts of mouse molars, we performed confocal microscopy analysis of the first molars of $DSPP^{Cerulean}/DMP1^{Cherry}$ mice.[23] This mouse strain enables the visualization of odontoblast bodies and processes through the dual expression of fluorescent proteins constitutively expressed under the DSPP (cerulean) and DMP1 (cherry) promotors. Three-dimensional confocal analysis of the first molars showed an entirely diverse structure of OPs in the crown and root part of the tooth (Fig. 1*A–C*). Processes in tooth crown dentin displayed smooth and straight morphology with thin and short secondary processes (branches of the main process). On the other hand, odontoblasts' processes in root dentin displayed complicated irregular morphology with longer and more pronounced secondary processes (Fig. 1*B, C*). To uncover if this phenomenon is also mirrored in the crown and root analogue of continuously growing teeth, we performed the same type of analysis in mouse incisors. Our analysis confirmed a consistent trend between processes found in both molar and incisor (Fig. 1*D–F*), supporting the crown analogue/root analogue theory (Fig. 1*G*). Mandibular incisors are in contrast to maxillary incisors more widely used in research.[28,30,31] To assess if different site-specific microstructure is reflected in dentin in both morphologically different incisors, we compared both incisors via the same approach and found an identical microstructural pattern (Fig. 2).

Enamel-forming epithelium controls the morphology of OPs in adjacent dentin

To investigate the induction role of different kinds of dental epithelium during early stages of hard-tissue formation, we took advantage of $Spry2^{+/-};Spry4^{-/-}$ mice, which are known for the presence of ectopic enamel on the lingual side of the incisors.[24,25] In contrast to the wild-type mouse in which the ameloblast layer is only present on the labial side, $Spry2^{+/-}/Spry\ 4^{-/-}$ mice display ameloblast layer on both labial and lingual sides. Additionally, the lingual cervical loop (LiCL) displays similar

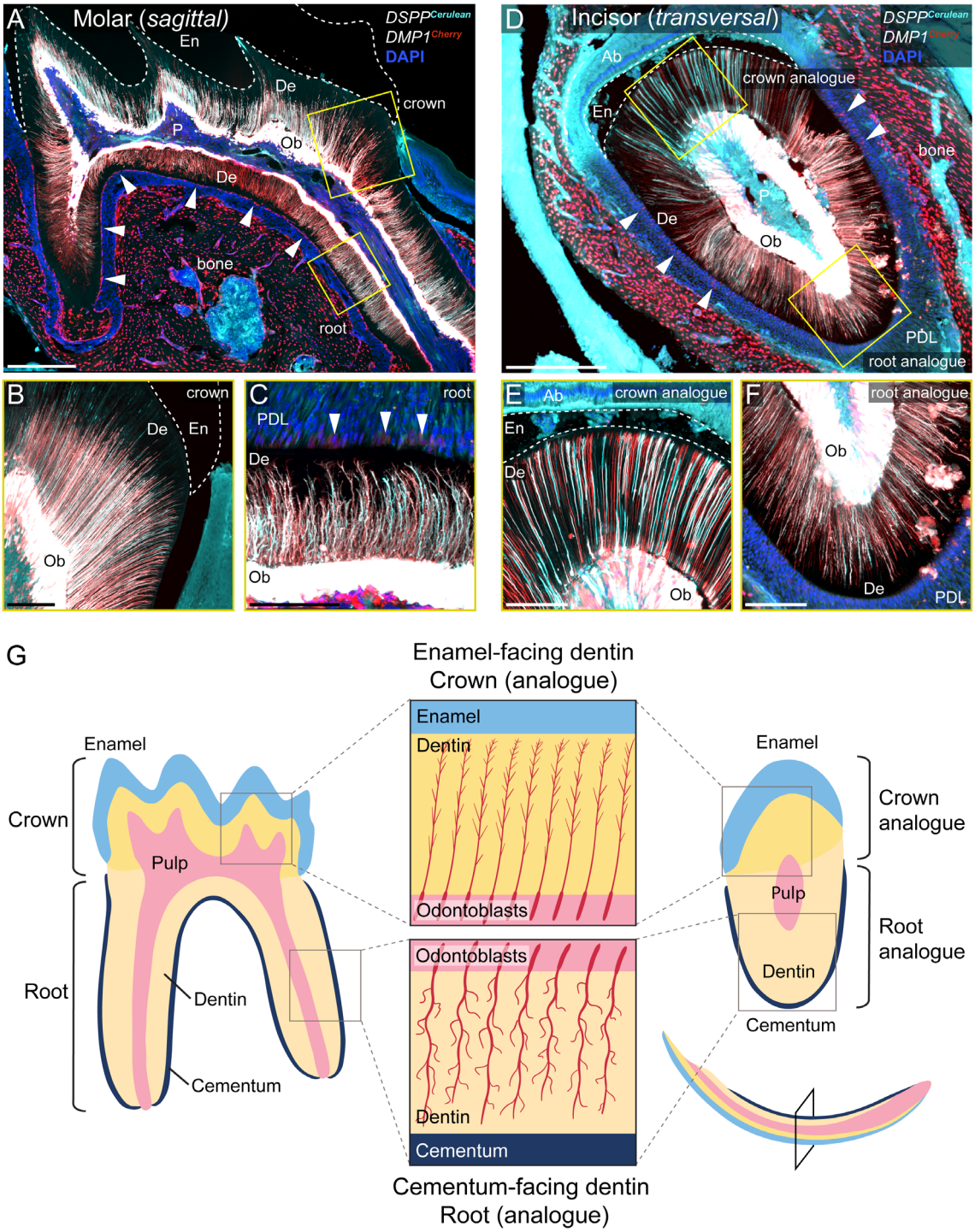

Fig 1. Dentin microstructure in molar and incisor: root (analogue) versus crown (analogue). Confocal images from thick, cleared histological sections from the *DSPP*^{Cerulean}/*DMP1*^{Cherry} mouse reporter strain show details of the microstructure of dentin with the focus on odontoblasts' processes in different parts of teeth. The sagittal section of the first molar (*A*) and transversal section of the mandibular incisor (*D*) show the structural similarities between these two types of teeth and the distribution of fluorescent proteins in the dental tissue and its close surroundings. Note the expression of *cherry* (DMP1) in odontoblasts but also bone-forming osteoblasts(cytes) and cementum-forming cementoblasts(cytes) on the surface of roots, while cerulean (DSPP) is expressed specifically by odontoblasts. Subsets of *A* and *B* show details of enamel-facing (crown/crown-analogue) dentin (*B*, *E*) and cementum-facing (root/root analogue) dentin (*C*, *F*), respectively. Arrowheads highlight the presence of DMP1-expressing cementum-forming cells located around the root of molar and root analogue of incisors. Schematic visualization of the microstructure of dentin showing the same pattern in enamel-facing and cementum-facing aspects in both molars and incisors (*G*). Scale bars = 300 μm (*A*, *D*), 100 μm (*B*, *C*, *E*, *F*). Ab = alveolar bone; De = dentin; en = enamel; Ob = odontoblasts; P = pulp.

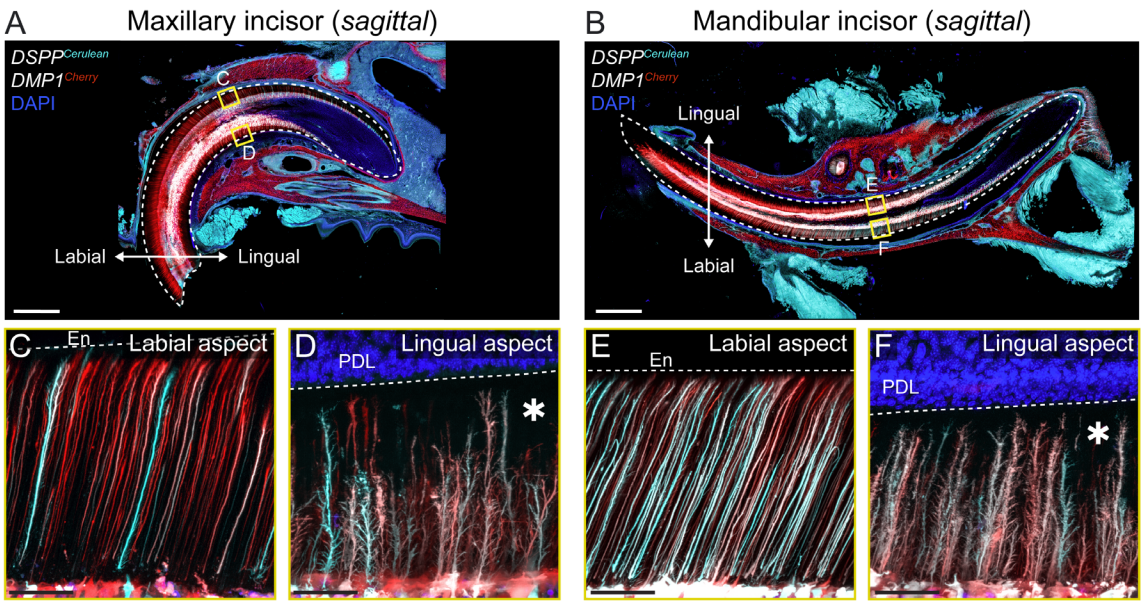

Fig 2. Mandibular and maxillary incisor dentin microstructure. Both upper and lower continuously growing incisors (*A*, *B*) show the same pattern in the labial (enamel-facing) (C, E) and lingual (cementum-facing) (D, F) odontoblast processes, respectively. White asterisks mark different microstructure of odontoblast processes in the lingual (cementum-facing) aspect of both mandibular and maxillary incisors. Scale bars = 1000 μm (*A*, *B*) and 50 μm (*C*–*F*) for details. En = enamel; PDL = periodontal ligaments.

morphology to the labial cervical loop (LaCL) (Fig. 6*C*, *D*); however, wild-type mice have an ameloblast layer only on the labial side and the lingual dental epithelium is disintegrated.[11] To visualize the morphology of OPs, we used the staining with Phalloidin-Alexa488, which specifically binds to actin[32] and enables the visualization of all cellular compartments in mineralized tissues. Confocal analysis of the phalloidin-stained sections from wild-type animals further confirmed the different structure of odontoblasts' processes in the labial and lingual aspects of the incisor (Fig. 3*A*), which coincided with our previous analysis of the $DSPP^{Cerulean}/DMP1^{Cherry}$ strain (Fig. 1*D*–*F*; Fig. 2). However, in the $Spry2^{+/-};Spry4^{-/-}$ animals, where the ectopic ameloblast layer and enamel are also developed on the lingual aspect, the microstructure of OPs was the same as on the labial aspect of the incisor (Fig. 3*A*, *B*), displaying the same smooth and straight morphology. Their appearance, therefore, reflected the morphology of the OPs in the crown dentin of the molar (Fig. 1*A*, *B*). To further analyze differences in the morphology of OPs and specifically their terminal branching regions,[14] which are in contact with adjacent enamel or cementum, we first performed detailed microscopy focusing on the terminal part of OPs (Fig. 4*A*). Furthermore, we performed the segmentation of the processes and quantified their straightness (Fig. 4*B*, *C*).

Our results show similarities in the pattern among the OP endings (Fig. 4*A*) and whole-process morphology (Fig. 4*B*) in the enamel-facing dentin and cementum-facing dentin. These results are consistent in wild-type molars, maxillary, and mandibular incisors, using $DSPP^{Cerulean}/DMP1^{Cherry}$ animals or phalloidin staining in wild-type and $Spry2^{+/-};Spry4^{-/-}$ animals (Fig. 4). The morphology of OPs in all enamel-facing dentins was highly similar. In the case of cementum-facing dentins, OPs in both maxillary and mandibular incisors displayed highly similar morphology. In the molars, OPs in the cementum-facing dentin displayed thinner and more twisting morphology when compared with the incisors (Fig. 4*A*).

To uncover the morphology and distribution of cementum-forming cherry^{+} (DMP1-expressing) cells in maxillary and mandibular incisors and to compare this pattern to molar roots, we analyzed the periodontal space on the lingual aspects of both types of incisors using $DSPP^{Cerulean}/DMP1^{Cherry}$ mouse strain (Fig. S1). Our data show that the structure of periodontal space on the labial aspect of the incisor resembles the situation in the molar. However, in the more distal parts, just a seldom presence of DMP1-expressing cementoblasts was observed. This enabled us to establish universal terms cementum-facing and enamel-facing dentin.

Quantifications of labial and lingual dentin differences

To quantify these differences, we performed segmentation and analysis of the individual processes. Quantification of processes' straightness shows that in the $DSPP^{Cerulean}/DMP1^{Cherry}$ strain's molar crown dentin, OPs display the mean straightness of 0.96 ± 0.02 (a straight line has the straightness of 1), while the OPs in the root dentin display the straightness of 0.90 ± 0.04 (Fig. 4*C*). OPs in the labial (with enamel) dentin of mandibular incisor display the straightness of 0.99 ± 0.01 and the OPs on the lingual (without enamel) side display 0.98 ± 0.01. In the maxillary incisor, the OPs of the labial (enamel-facing) side showed the straightness of 0.98 ± 0.01, while on the lingual (cementum-facing) side, OPs displayed 0.95 ± 0.02. In the wild-type maxillary incisor stained with phalloidin, OPs of the labial side displayed the straightness of 0.98 ± 0.01. The OPs on the lingual side displayed, on the other hand, the straightness of 0.90 ± 0.05. Finally, the OPs of the $Spry2^{+/-};Spry4^{-/-}$ animals displayed on the labial (enamel-facing) side the straightness of 0.99 ± 0.01 and 0.99 ± 0.00 on the lingual (ectopic enamel-facing) side.

To further highlight the differences in the features of odontoblast processes and corresponding dentins, we analyzed confocal images of labial (enamel-facing) and lingual (cementum-facing) dentins of wild-type animals and labial (enamel-facing) and lingual (ectopic enamel-facing) dentins of *Spry2*$^{+/-}$;*Spry4*$^{-/-}$ animals (Fig. 5). The analysis of OP's width showed that processes localized on the labial-side dentins of wild-type mice (both mandibular and maxillary) and maxillary *Spry2*$^{+/-}$;*Spry4*$^{-/-}$ incisors were significantly thinner ($p < 0.0001$) than the processes located in the corresponding lingual-side dentins (Fig. 5*A*). Interestingly, the width of the OPs located in the lingual (ectopic enamel-facing) dentin of the *Spry2*$^{+/-}$;*Spry4*$^{-/-}$ maxillary incisor was significantly lower compared with its lingual wild-type counterpart (Fig. 5*A*).

Analysis of the number density of the processes showed that the processes on the labial sides of the incisors have significantly higher density than processes on the lingual side of all analyzed conditions, including the ectopic enamel-facing lingual dentin of *Spry2*$^{+/-}$;*Spry4*$^{-/-}$ animals (Fig. 5*B*). Comparison of wild-type and *Spry2*$^{+/-}$;*Spry4*$^{-/-}$ process density showed no significant change ($p = 0.0532$) between the lingual sides of the incisors.

To quantify the changes of the dentin quality in relation to the OPs, we analyzed the relative fraction of dentin height without the presence of the main process (Fig. 5*C*) and the distribution of all processes in different types of dentins (Fig. 5*D*). The fraction of the dentin without the presence of the main process was significantly larger ($p < 0.0001$) in the lingual (cementum-facing) dentin than in the labial (enamel-facing) dentins of wild-type mandibular and maxillary incisors. In contrast to this, the fraction of the labial and lingual dentins of the maxillary incisor of the *Spry2*$^{+/-}$;*Spry4*$^{-/-}$ animals showed similar values ($p < 0.7462$), which fully reflects the altered situation in the lingual (ectopic enamel-facing) dentin and show high similarity induced by the changed type of dental epithelium. The differences between the lingual sides of maxillary incisors of wild-type and *Spry2*$^{+/-}$;*Spry4*$^{-/-}$ animals were also significant (Fig. 5*C*).

To quantify the density and distribution of all OPs (including side branches) in the enamel-facing and cementum-facing dentins, we analyzed the OP density in 10 different regions, beginning at the predentin up to the outermost dentin (Fig. 5*D*; Fig. S2). Pearson's correlation between the lingual and labial dentins was calculated using medians of each of the data points (Fig. 5*D*). Our analysis shows distinct trends of the area fraction in labial and lingual dentin of mandibular ($R = 0.6165$, $p = 0.0802$) and maxillary ($R = 0.2612$, $p = 0.46$) incisors of wild-type animals. In contrast to wild types, the analyses of labial and lingual dentins in *Spry2*$^{+/-}$;*Spry4*$^{-/-}$ maxillary incisor show correlating trends ($R = 0.8697$, $p = 0.0011$), which further confirms our hypothesis about the inductive function of the type of attached dental epithelium during development. The plots of Pearson's correlations are shown in Fig. S3.

All performed quantifications further support our hypothesis of the different microstructure of cementum-facing and enamel-facing dentin. Most interestingly, the lingual, ectopic enamel-facing dentin of the *Spry2*$^{+/-}$;*Spry4*$^{-/-}$ animal displayed similar patterns of OPs compared with its labial counterpart. This confirms a different inductive role of ameloblast-forming dental epithelium and non-ameloblast-forming dental epithelium on adjacent dentin microstructure.

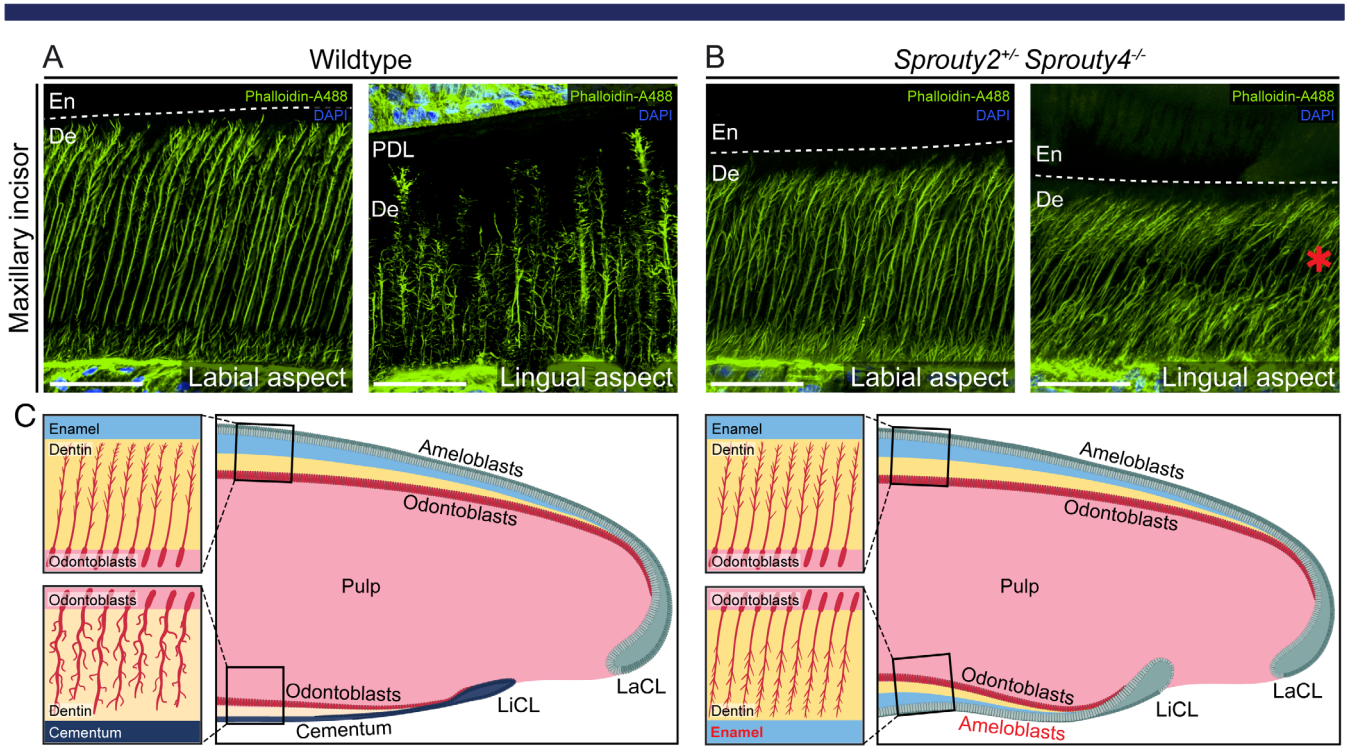

Fig 3. Dentin adjacent to ectopically developed enamel shows altered microstructure. Confocal images of the labial and lingual aspect of maxillary incisors stained with Phalloidin-Alexa488 show the different microstructure of OPs on the labial and lingual aspect of incisor in wild-type animals (*A*) and similar microstructure on both aspects in maxillary incisor of *Spry2*$^{+/-}$;*Spry4*$^{-/-}$ animals (*B*) having ameloblasts and enamel on both sides of the tooth. (*C*) Schematic drawing reflecting the influence of different dental epithelium on dentin development. Red asterisk shows the altered morphology of OPs in dentin adjacent to ectopic enamel on the lingual aspect of the maxillary incisor in *Spry2*$^{+/-}$;*Spry4*$^{-/-}$. Scale bars = 50 μm. En = enamel space; LaCL = labial cervical loop; LiCL = lingual cervical loop; PDL = periodontal ligament.

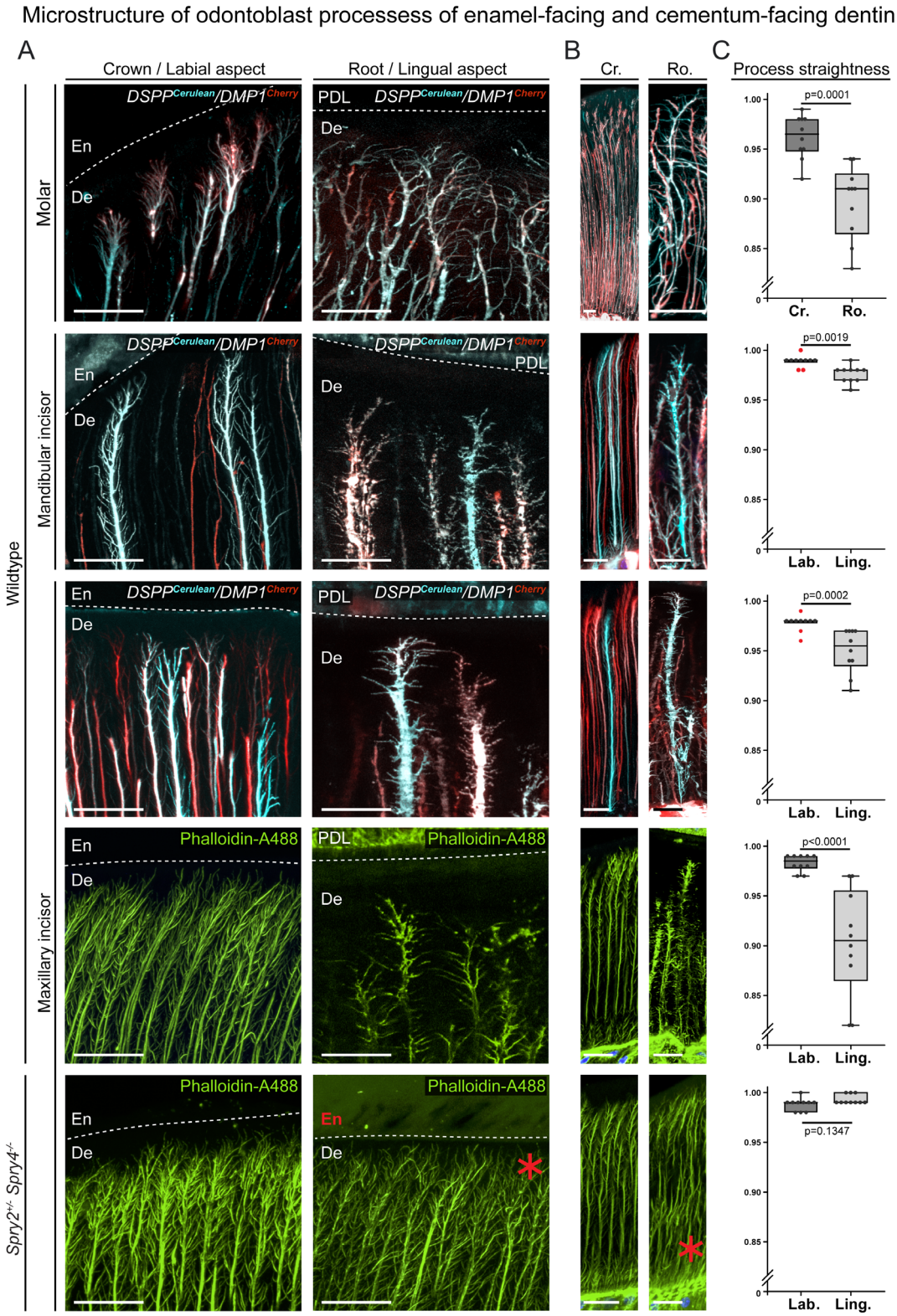

Fig 4. Analysis of odontoblasts' terminal branching regions and processes straightness in enamel-facing and cementum-facing dentin. Confocal images of histological sections from *DSPP*^{Cerulean}/*DMP1*^{Cherry}, wild-type, and *Spry2*$^{+/-}$;*Spry4*$^{-/-}$ animals stained with Phalloidin-Alexa488 with a special emphasis on the terminal branching regions relating to the first formed dentin adjacent to enamel and cementum, respectively (*A*). Details on the process morphology are shown in (*B*) and quantifications straightness of the processes in (*C*). Red asterisks show the altered morphology of OPs in dentin adjacent to ectopic enamel on the lingual aspect of the maxillary incisor in *Spry2*$^{+/-}$;*Spry4*$^{-/-}$. Scale bars = 20 μm. Cr = crown (analogue); en = enamel/enamel space; Lab. = labial side; Ling. = lingual side; PDL = periodontal ligament; Ro = root (analogue).

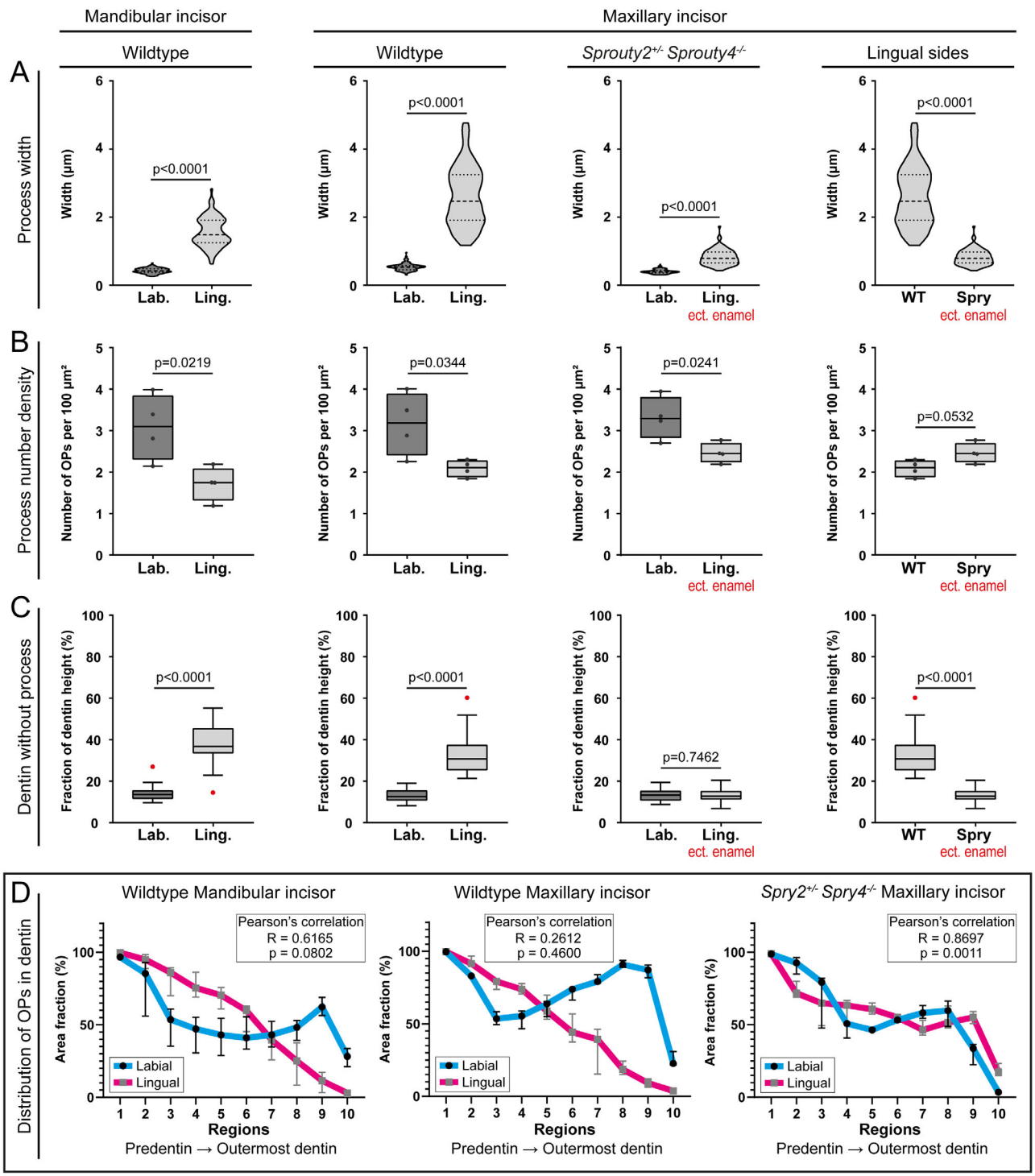

Fig 5. Characterization of the features of processes and dentin. Quantification of different aspects of odontoblast processes and dentin quality in mandibular wild-type and maxillary wild-type and *Spry2*$^{+/-}$;*Spry4*$^{-/-}$ animals. Process width (*A*) measured as a width of individual odontoblast processes at the distance of 40 µm from the predentin-pulp edge ($n = 85$). Process density (*B*) calculated as a number of OPs per 100 µm^2 of dentin ($n = 4$ ROIs). Fraction of dentin height without the presence of the main process (*C*) ($n = 33$). Analysis of the distribution of all processes in dentin ranging from predentin (1) to the outermost dentin (10) is shown in (*D*). Pearson's correlation coefficients (*R*) were calculated and tested. $p < 0.05$ expresses the fact that trends are correlated ($n = 3$ ROIs for each data point). Ect. enamel = ectopic enamel; Lab. = labial side; Ling. = lingual side.

Early polarization and differentiation of odontoblasts in enamel and cementum-facing dentin

To further investigate an early odontoblast's differentiation and dentin morphogenesis, we analyzed the (pre)odontoblast-epithelium interphase close to the labial and lingual cervical loops in wild-type and *Spry2*$^{+/-}$;*Spry4*$^{-/-}$ animals (Fig. 6). We show that the presence of differentiating preameloblasts stimulates adjacent preodontoblasts to synchronous polarization and more consistent generation of OPs, resulting in the generation of highly tubular dentin (Fig. 6*A*, *C*, *D*). Conversely, the emerging dentin adjacent to the lingual aspect of the wild-type incisor shows almost atubular structure, likely resulting from more asynchronous polarization of odontoblasts suggested by the uneven distribution of odontoblast nuclei (Fig. 6*B*). These findings suggest an early patterning effect of the adjacent dental epithelium type on the future microstructure of the whole dentin matrix.

To investigate differences in the timing of odontoblast differentiation between the labial and lingual side of the tooth, we measured the distance of first DSPP- and/or DMP1-expressing (cerulean and cherry fluorescent protein-expressing, respectively) odontoblast from the apex of each cervical loop in *DSPP*^{Cerulean}/*DMP1*^{Cherry} animals (Fig. 7). In the mandibular incisor, the distance to the first cerulean-positive, cherry-positive, and both reporter-expressing odontoblast was significantly longer on the lingual side when compared with the labial side (Fig. 7*A*, *B*). In the maxillary incisor, the differences in the distances were greatly reduced, but the distances on the lingual side were still significantly longer for all three measured features (Fig. 7*C*, *D*). These data suggest that the differentiation into functional odontoblasts is faster on the labial side of the incisor.

Molecular differences of odontoblasts on the labial and lingual aspect of mouse incisor

To address molecular differences of odontoblasts on the labial and lingual aspect, we performed in situ hybridization (ISH) and immunohistochemical (IHC) expression analysis of selected odontoblast-specific genes. First, we analyzed the expression of two Wnt-signaling related genes, *Dkk1* and *Wisp1*, using ISH.

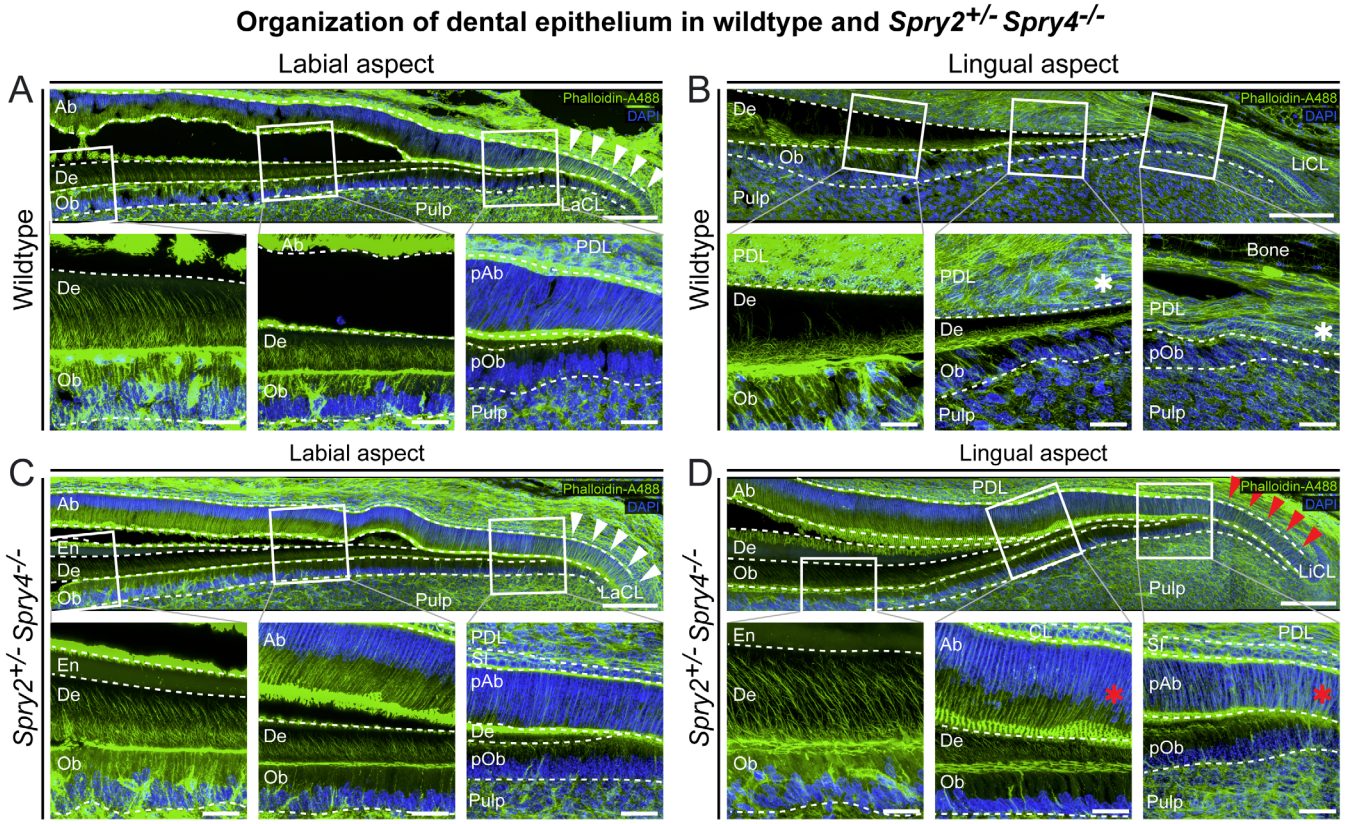

Fig 6. Early polarization of odontoblast and dentin patterning. Confocal images of histological sections from maxillary incisors of wild-type and *Spry2*$^{+/-}$;*Spry4*$^{-/-}$ animals stained with Phalloidin-Alexa488 (green) and DAPI (blue). Each panel contains an overview image of the early differentiating area where preodontoblasts polarize and differentiate. Highlighted subsets show details of differentiation. In the wild-type mouse, epithelium at the labial aspect gives rise to (pre)ameloblasts (highlighted with white arrowheads *A*), whereas at the lingual aspect, preameloblasts are not formed and the epithelium is being disintegrated (*B*). In contrast to this, the enamel-forming ameloblast epithelium is formed by both labial and lingual cervical loops of *Spry2*$^{+/-}$;*Spry4*$^{-/-}$ incisors. Ectopic, (pre)ameloblastic epithelium is marked with red arrowheads. Asterisks highlight the difference between the structure of wild-type and *Spry2*$^{+/-}$;*Spry4*$^{-/-}$ lingual cervical loop highlighting different interacting partners of the respective (pre)odontoblasts. Note faster polarization of odontoblasts induced by adjacent epithelium with ameloblasts at the labial aspect of wild-type and both aspects of *Spry2*$^{+/-}$;*Spry4*$^{-/-}$ incisors (*A*, *C*, *D*). Scale bars = 100 μm (cervical loop tile scans), 25 μm (details). Ab = ameloblasts; pAb = preameloblasts; De = dentin; En = enamel space; LaCL = labial cervical loop; LiCL = lingual cervical loop; Ob = odontoblasts; pOb = preodontoblasts; P = pulp; PDL = periodontal ligament.

Strong expression of *Dkk1* was localized in preodontoblasts exclusively on the labial side of the incisors (Fig. 8*A*, *B*). On the lingual side, only weak spots of positive signal were found. *Wisp1* expression was also located predominantly on the labial side of the incisors with the expression being consistent even in older odontoblasts (Fig. 8*C*, *D*). On the lingual side, a weaker signal was found only close to the cervical loop. Similar to this, we observed a specific and strong nuclear signal of SALL1 (IHC) in the odontoblasts on labial sides of the incisors (Fig. 8*E*, *F*). On the lingual side, the nuclear signal of Sall1 was only slightly above the level of the background and started further from the cervical loop apex. Nuclear signal of NFIC was found in the pulp cells surrounding both cervical loops (Fig. 8*G*, *H*). NFIC was also expressed in odontoblasts and subodontoblastic cells on both sides of the incisors. The signal found in odontoblasts did, however, diminish further from the cervical loops.

Analysis of element composition and dentin density

To further investigate whether the differences in the morphology of the OPs are connected to the different composition of key elements of the dentin matrix, we performed laser-induced breakdown spectroscopy (LIBS) analysis on the established model of mouse incisor. The spectroscopic analysis provided semiquantitative information on the spatial distribution of calcium and magnesium in mandibular and maxillary mouse incisors on transversal sections. The methodology of elemental mapping by LIBS has been previously described.[33,34] The analysis was performed on the ground, polished sections from the distal part of the maxillary and mandibular incisors (Fig. 9*A*).

The relative contents of calcium and magnesium were plotted as a function of the measurement position. It was observed that calcium was most abundant in the enamel in contrast to magnesium, which was detected in higher amounts in dentin (Fig. 9*A*). Focusing on the dentin, we detected a higher amount of calcium in the dentin facing the enamel in both mandibular and maxillary incisors. Magnesium showed uneven distribution within the dentin matrix being slightly more present in the enamel-facing dentin in the mandibular incisor.

Additionally, principal component analysis (PCA) of the LIBS data was performed to further highlight more complex relationships of the elemental composition of incisors. The utilization of PCA in LIBS has already been thoroughly described previously.[35] Principal component (PC) scores were plotted on a map with respect to the original spectra position. The resulting patterns were afterwards compared with the original teeth structure knowing the correlation between PC scores and the original samples. The respective PC loadings were investigated to yield information about the contribution of individual elements. Most interesting information was observed in PC1 and PC3 presented in Fig. 9*B* and Figs. S3 and S4. Analysis of loadings (Fig. S4) showed the highest contribution of Ca followed by Mg to PC1. In other words, the higher the PC score means the higher the intensity of the spectral line and hence the content of the respective element. Conversely, in PC3, higher values resulted from the high intensity of calcium and low intensity of magnesium. PCA suggested a trend of enamel-facing dentin being different in

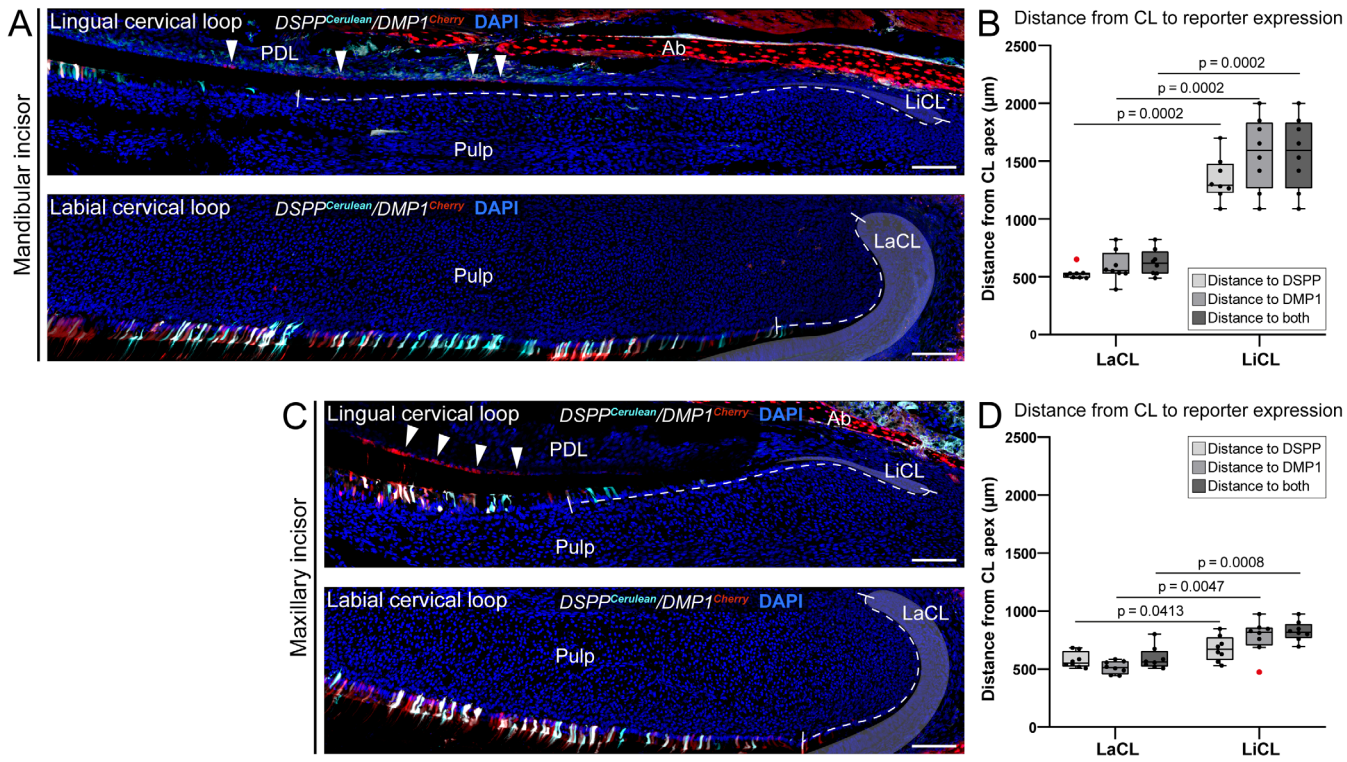

Fig 7. Reporter expression distance analysis. Analysis of images taken from *DSPP*^{Cerulean}/*DMP1*^{Cherry} mandibular (*A*) and maxillary (*C*) incisor's apical regions. The distance from the apex of the cervical loop to the first cell expressing fluorescent protein: DSSP (cerulean), DMP1 (cherry), or both were measured and results were compared between the lingual and labial aspects (*B*, *D*). Scale bars = 200 µm. Arrows indicate cementoblasts. Ab = alveolar bone; LaCL = labial cervical loop; LiCL = lingual cervical loop; PDL = periodontal ligament.

elemental composition from the opposing, cementum-facing dentin (Fig. 9*B*; Fig. S4). This phenomenon was more pronounced in the case of the mandibular incisor.

Based on the above-mentioned results, the PC1 and PC3 scores were cross plotted (Fig. S4) and data points clustered by using *k*-means clustering (5 clusters). Each cluster was assigned a color and the respective colors were subsequently presented in the picture as a function of position (Fig. 9*C*). Cluster 1 corresponds to enamel, clusters 2 and 3 correspond to both cementum-facing dentin and alveolar bone. Cluster 5 corresponds to resin in which the samples were embedded and soft tissues. Finally, cluster 4 specifically designates enamel-facing dentin.

Finally, to assess the dentin X-ray density in different regions of dentin, we utilized the micro-CT analysis of wild-type maxillary

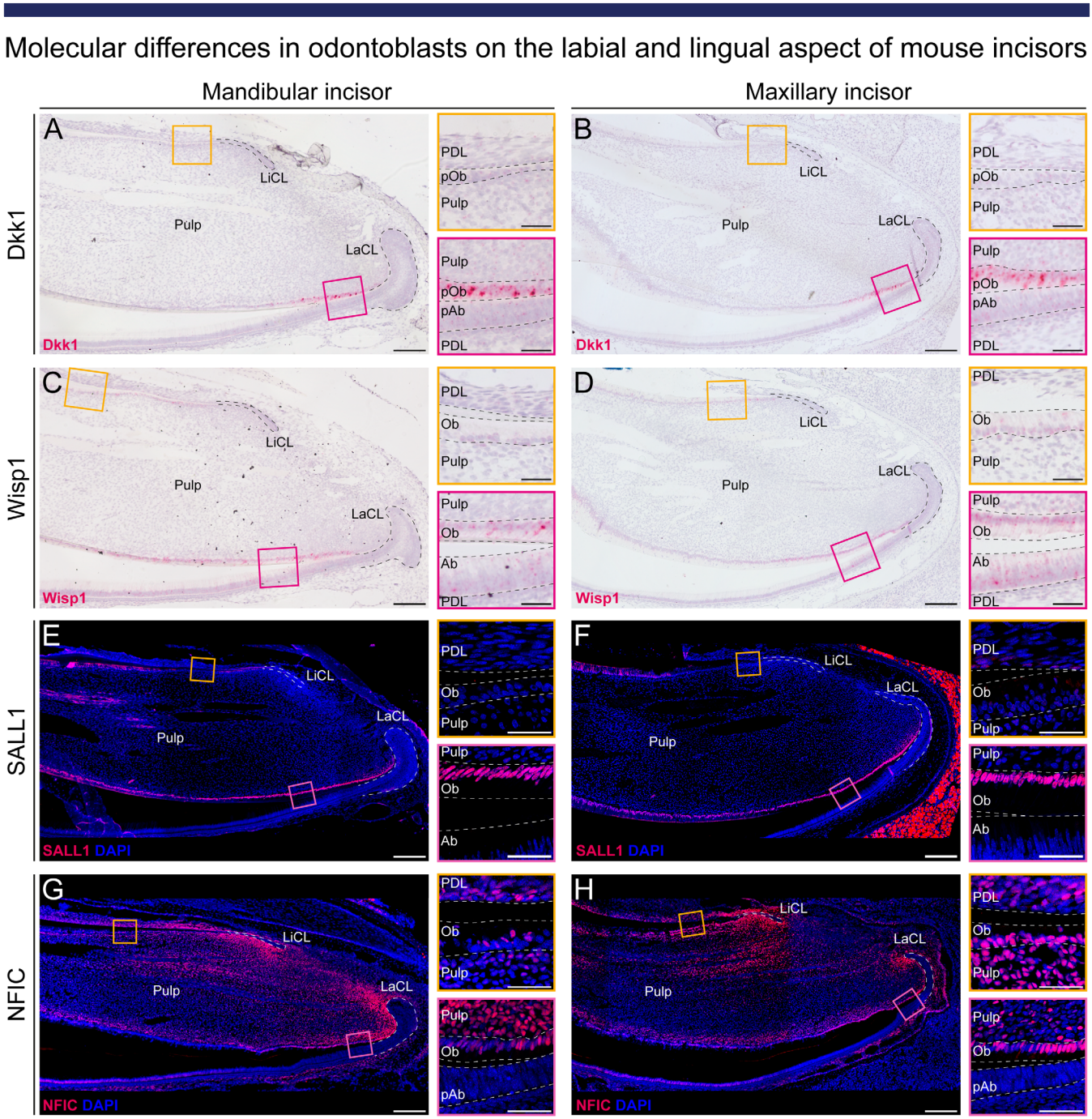

Fig 8. Molecular differences of odontoblasts on the labial and lingual aspect of mouse incisor. Analysis of selected odontoblast-specific molecular markers shows a different expression pattern on the labial and lingual aspect of both mandibular and maxillary incisors. In situ hybridization of *Dkk1* (*A*, *B*) and *Wisp1* (*C*, *D*) shows a specific expression only in odontoblasts on the labial aspect of the incisor. Similar to this, the immunohistochemical staining of SALL1 shows the same expression pattern (*E*, *F*), while the immunohistochemical staining of previously shown NFIC (*G*, *H*) did not show a different expression on labial and lingual aspects. Scale bars = 200 μm (overview images) and 50 μm (details). LaCL = labial cervical loop; LiCL = lingual cervical loop; Ab = ameloblasts; pAb = preameloblasts; Ob = odontoblasts; pOb = preodontoblasts; PDL = periodontal ligament.

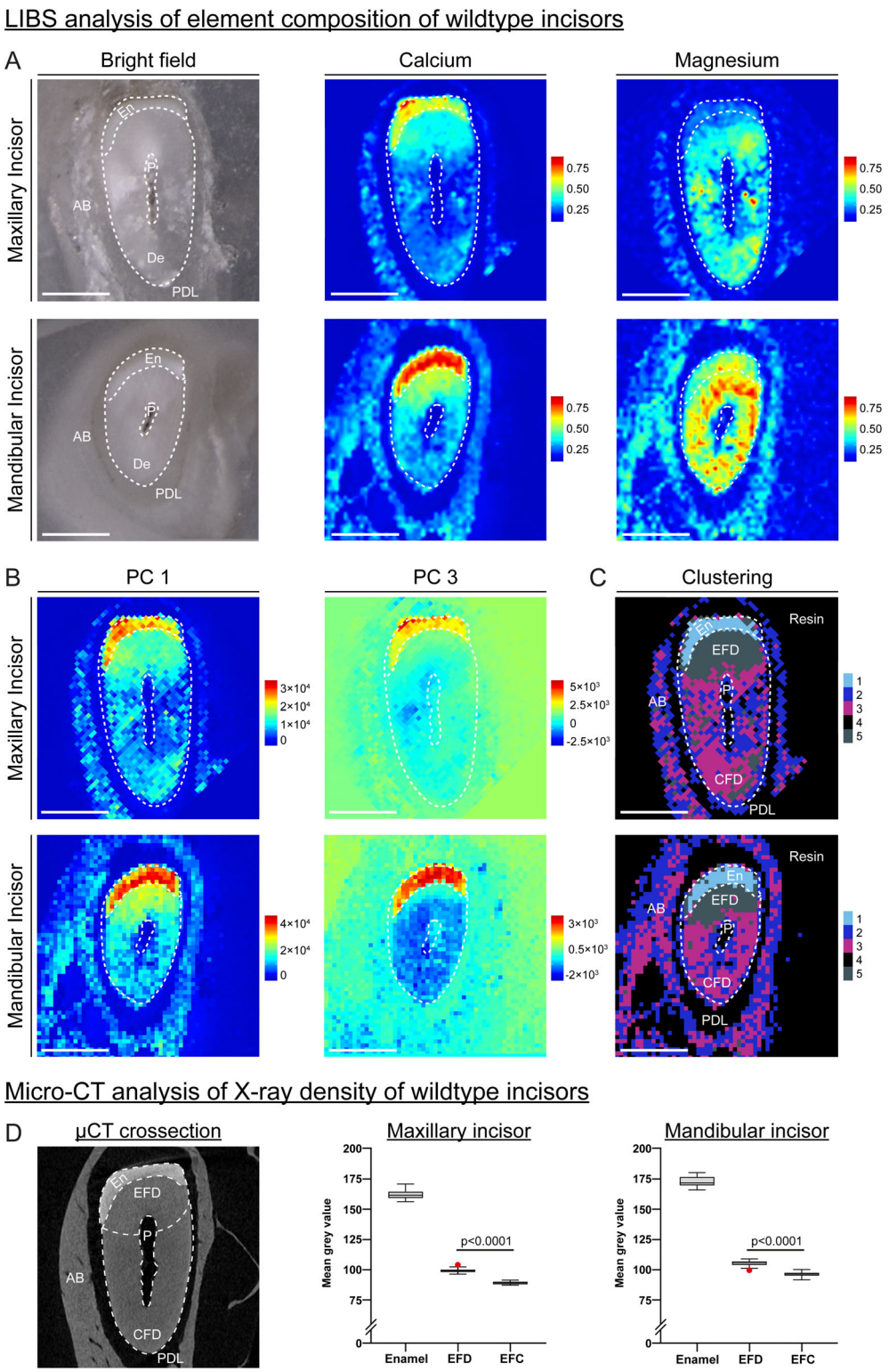

Fig 9. Analysis of elemental composition and dentin density. Brightfield images (left) of ground sectioned, polished teeth sections and subsequent analyses (right) represent heat maps showing the relative amount of calcium and magnesium on the transversal section from the distal part of the mandibular and maxillary incisor (*A*). The function of position plots of principal component analysis (*B*) and *k*-means clustering from the PCA (*D*). Micro-CT analysis of dentin density in EFD and CFD of mandibular and maxillary incisors (*C*) ($n = 25$). Graphs also plot the grey mean values of enamel to enable the comparison between dentin and enamel. Scale bars = 500 µm. AB = alveolar bone; CFD = cementum-facing dentin; EFD = enamel-facing dentin; En = enamel; PDL = periodontal ligament.

and mandibular incisor (Fig. 9*D*). Although the differences between the enamel-facing (EFD, labial) and cementum-facing (CFD, lingual) dentins are faint, the analysis of mean gray value of these two regions has shown significantly higher values in EFD ($p < 0.0001$) in both mandibular and maxillary incisor.

Discussion

Microstructure, chemical composition, and development of dentin and odontoblasts have been extensively studied topics for many decades. This tissue gives the tooth its shape and specific mechanical and sensory properties. Here we expand the knowledge about dentin microstructure and composition and provide evidence for differences in the microstructure of dentin secreted by odontoblasts facing dental epithelium during early hard-tissue formation. Furthermore, we show differential expression of several odontoblast-specific genes that may control the observed differences in dentin and odontoblast structure.

Because dentin is not remodelled, the complete developmental history of dentin is sealed in the inner structure of this hard matrix. The morphology of dentinal tubules then reflects the development of odontoblasts and visualization of dentin microstructure provides us with a detailed history of the dentinogenesis itself.[14,36] Our data show that the type of dental epithelium influences the adjacent preodontoblasts in a different manner, which results in different microstructure and elemental composition of the adjacent dentin controlled by the very beginning of its formation.

It was shown before that dentin in root and crown differs on several levels including the composition of phosphoproteins, levels of calcification, speed of crystal growth, and mechanical properties.[18,19,37] However, only a limited number of research studies focus on the morphology of the dentinal tubules and their functional components—odontoblast processes.[14,36,38] Using *DSPP*^{Cerulean}/*DMP1*^{Cherry} mouse strain, we were able to map the three-dimensional morphology of odontoblast processes in an unprecedented detail. First, we described a significantly different OPs morphology within the crown and roots of mouse molars. Furthermore, our results show that this phenomenon is reflected in the incisors, which are structurally and developmentally different. Importantly, we show that the inner microstructure of dentin is changed when the type of adjacent epithelium changes its function. Our findings suggest that the predetermination of dental epithelium controls the structure of OPs by controlling the differentiation of the adjacent odontoblasts. Our results are consistent when comparing different types of teeth (both molars and incisors) and different inbred strains (CD1 and Bl/6 background). Functional analysis on animals with ectopic enamel on the lingual aspect of maxillary incisors (using *Spry2*$^{+/-}$;*Spry4*$^{-/-}$ animals) enabled us to make a conclusion of enamel-facing and cementum-facing predetermination of dentin microstructure. Important to note is that the phenotype of *Spry2*$^{+/-}$;*Spry4*$^{-/-}$ animals is highly variable with incomplete penetrance. We observed the presence of ectopic enamel only in a few maxillary incisors (which were used for the analysis), but no mandibular incisors with ectopic enamel were observed. Comparing the microstructure of maxillary and mandibular incisors using *DSPP*^{Cerulean}/*DMP1*^{Cherry} animals provided us with identical results regarding the microstructure of OPs. This, together with the results obtained from the analysis of *Spry2*$^{+/-}$;*Spry4*$^{-/-}$ maxillary incisor, serves as adequate proof of principle.

It had been shown that cementum is present on the lingual aspect of rodent incisors.[39] The development of cementoblasts and cementum in continuously growing incisors is still not fully understood.[39-41] Our results confirm the presence of DMP1-expressing cementoblasts in the periodontal space attached to the lingual side of dentin. Periodontal ligaments in periodontal space were visualized by POSTN staining for greater clarity (Fig. S1).[28] The structure of the cementoblast layer and periodontal space in the incisors displayed the same pattern as in molar roots. This enabled us to establish universal terms cementum-facing and enamel-facing dentin. DMP1-expressing cementoblasts were preferentially found in the more apical region on the incisor lingual aspect. In the more distal parts, just a seldom presence of DMP1-expressing cementoblasts was observed. This might show that the activity of cementum-forming cells is limited mostly to the apical region and later their activity decreases.

To quantify the observed differences between the OPs found in enamel-facing and cementum-facing dentin, we at first chose straightness. This parameter was chosen because of its independence on the length of the process, which naturally varies because of changing dentin height. The observed trend showed that in the enamel-facing dentin, the OPs have straighter (straightness value closer to 1) morphology when compared with the cementum-facing dentin. Although the general trend of cementum-facing and enamel-facing microstructure of OPs was similar in all observed conditions and samples, minor differences can be observed in OP morphology comparing incisors and molars.

The overall larger differences in the straightness of the two different classes of OPs in the molar may be caused by the temporal separation of the production of the crown and root dentin. Conversely, the smaller differences in the incisors may be caused by synchronous deposition of the dentin matrix, which has to accommodate for the abrasion of the tip of the incisor. Furthermore, the small, though still statistically significant, differences between the OPs in the mandibular incisor may be in part caused by less pronounced curvature of the incisor when compared with the maxillary incisor in which the OPs have a larger difference between the two sides.

Moreover, in mouse incisors, we analyzed the OP's width, number density, the dentin quality by measuring the fraction of dentin height without the presence of the main process and the analysis of the distribution of all processes in different regions of dentin. All these data have consistently shown statistically significant differences in all aspects between the labial and lingual sides of wild-type mandibular and maxillary incisors. Additionally, the analysis of dentin in *Spry2*$^{+/-}$;*Spry4*$^{-/-}$ maxillary incisors has shown that dentin facing an ectopically present enamel on the lingual aspect of the incisor is in most of the observed aspects more similar to dentin on the labial side. This further confirms the inductive role of different kinds of dental epithelium on dentin microstructure. Interestingly, the number density of processes in *Spry2*$^{+/-}$;*Spry4*$^{-/-}$ displayed the same trend as observed in wild-type animals. This suggests that this feature of dentin is determined by a different mechanism, which is independent of the inductive role of the ameloblastic epithelium.

Previous studies performed on rat incisors report that in mandibular incisors the enamel-facing odontoblasts display production of predentin that exceeds that of the cementum-facing odontoblasts.[18] Furthermore, it has been reported that the conversion of cementum-facing predentin into dentin is faster than

in the enamel-facing dentin. Thus, the speed of dentin growth might cause a change of OP morphology as a secondary effect.

Based on these previous observations, we decided to investigate the possible differences in the early odontoblast differentiation and dentin production. To do so, we focused on the cervical regions of the incisors. Our results show that the distinct morphology of OPs on labial and lingual sides of wild-type incisors is established during the early odontoblast differentiation. Interestingly, on the lingual side, the odontoblasts polarize further from the cervical loop and only a few of them leave their processes in the newly formed dentin. This paired with the analysis of the relative fraction of dentin height without the presence of the main process suggests a more asynchronous differentiation of odontoblast without the presence of ameloblastic epithelium. This is further supported by the fact that in both analyses the *Spry2*$^{+/-}$;*Spry4*$^{-/-}$ lingual dentin displays the same trends as the labial dentin.

To further investigate the rate of differentiation of odontoblasts, we analyzed the expression of the reporters in *DSPP*^{Cerulean}/*DMP1*^{Cherry} mice. Our results go in line with the aforementioned trends. Odontoblasts on the lingual side start to express *Dspp* and *Dmp1* further from the cervical loop, which suggests slower odontoblast differentiation in the absence of ameloblastic epithelium.

Although we observed a consistent phenotype in all analyzed features and conditions, the precise molecular signalling responsible for a different dentin production and microstructure is, however, still unknown. One of the mechanisms that might have a role in this process is RUNX2 and Wnt signalling, which has been shown to have a differential role and effect on adjacent dental mesenchyme in the crown and root dental epithelium.[42] Our results support these findings and suggest that Wnt signalling likely plays an important role in dentin patterning. Two Wnt pathway-related genes (*Dkk1* and *Wisp1*) showed robustly different expression patterns in odontoblasts on the labial and lingual aspects of mouse incisor. Moreover, SALL1, a newly identified transcription factor present during odontoblast development,[28] showed the same pattern and was predominantly expressed in odontoblasts on the labial side. Recently, SALL1 has been found to be an interacting partner of RUNX2 and was shown to increase the accessibility of cis-regulatory elements inside the *Runx2* locus.[43] Interestingly, the knockdown of *Sall1* in murine dental pulp cells in vitro have reduced their odontoblastic differentiation and also inhibited calcification.[43] This might coincide with the slower odontoblast differentiation and reduced amount of calcium in the lingual dentin and also its lesser X-ray density in vivo.

Even though it was previously shown that NFIC plays an important role in dental mesenchyme during the growth of molar roots,[44-46] we did not observe a clear difference in the expression of this protein on the labial and lingual side of mouse incisor, suggesting it has a different role in incisor renewal than in the extensively studied molar development.[44-46] Further investigation needs to be performed to answer precise molecular pathways controlling divergent dentin development.

To investigate the elemental composition of the calcified matrix in each type of dentin, we performed LIBS analysis focused on calcium and magnesium content. We uncovered characteristic regionalization of these two elements distinguishing a cementum-facing and enamel-facing dentin on the elemental level. Previous studies, which used microindentation as one of the methodologies, suggested that in the rat incisor, the enamel-facing dentin is harder, which is caused by a higher amount of calcium and lower amount of magnesium and vice versa for the cementum-facing dentin.[47] It has been further connected to the fact that the enamel-facing dentin matrix displays larger calcospherites, which result from slower calcification, which is likely regulated by the larger ratio of highly phosphorylated phosphoproteins. Cementum-facing dentin then displays smaller calcospherites, resulting from faster calcification likely regulated by a larger ratio of slightly phosphorylated phosphoproteins.[47] Authors then attribute the higher amount of magnesium in the cementum-facing dentin as a result of faster calcification, which produced apatite with lower purity (polluted with magnesium).[18,19,37] Contrary to the research performed on the rat model, we have found that in the mouse mandibular incisor, the intensity of magnesium signal is slightly elevated in the enamel-facing region of the tooth, and thus reflecting the distribution of calcium, which was, however, much more distinct. In the case of the maxillary incisor, magnesium was more evenly distributed, and its signal displayed lesser intensity compared with the mandibular incisor. The calcium distribution in the maxillary incisor, however, precisely reflected the calcium distribution in the mandibular incisor and therefore was more concentrated in the enamel-facing dentin. Additionally, we employed PCA analysis and *k*-means clustering of the PCA scores. PCA can reveal differences in multidimensional data, express the difference numerically (by scores of respective principal components), and describe the importance of each part of multidimensional data for a particular principal component (PC). In our case, by employing the PCA, we were able to discriminate specific parts of the transversal section of mouse teeth not only based on the relative change of selected elements but also on their complex relationship. The PCA plots and the *k*-means clustering obtained from the PCA data, therefore, highlight the fact that the labial and lingual dentins are distinct when it comes to the composition of the two important elements. Our findings concerning the X-ray density of labial and lingual dentins go in line with previous work on the topic, as it was previously shown that root dentin is less dense than the average value of dentin density.[48,49]

Taken together, we summarize that the distinct inner structure of dentin is, from the very beginning of its development, controlled by the type of the adjacent epithelium, and we hypothesize that it is responsible for the different mechanical properties of dentin. Our data also suggest that the different dentin microstructure is controlled by Wnt signalling in odontoblasts. This new insight into the connection between dentin development, function, structure, and composition will be important for future research focused on dental patterning or organogenesis based on epithelial-mesenchymal interactions.

Disclosures

All authors state that they have no conflicts of interest.

Acknowledgments

JK was supported by the Grant Agency of Masaryk University (MUNI/H/1615/2018) and by funds from the Faculty of Medicine MU to junior researcher. JL was supported by the Grant Agency of Masaryk University (MUNI/IGA/1532/2020) and is a Brno PhD Talent Scholarship Holder, funded by the Brno City Municipality. MH and KS were supported by the Grant Agency of the Czech Republic (21-04178S). PP gratefully acknowledges the support

of the Czech Grant Agency under the project 20-19526Y. MH, KS, and MB were supported by Charles University and the Czech Ministry of Education, Youth and Sports (Progres Q25 and Q29).

We thank Adela Lochmanova for her help taking care of the mice colony and Katarina Mareckova for her help with histological analysis. Our special thanks go to Karel Novotny (Faculty of Science, Masaryk University) and Anna Konecna (CEITEC, Brno University of Technology), who helped with the initial LIBS analysis, and Petr Zaunstöck (Faculty of Science, Masaryk University) for his help with the polishing of samples used for LIBS analysis. Furthermore, we also thank Daniel Kovac for his help with statistical analysis. We acknowledge the core facility CELLIM of CEITEC supported by the Czech-BioImaging large RI project (LM2018129 funded by MEYS CR) for their support with obtaining scientific data presented in this paper.

Authors' roles: JKr planned and performed experiments, analyzed the data and wrote the manuscript. JL performed experiments, analyzed the data and wrote the manuscript. MK, DP, VL, MGL, KS, MB, AV, PP, MH, MM performed experiments and analyzed the data. JKa analyzed data.

Peer Review

The peer review history for this article is available at https://publons.com/publon/10.1002/jbmr.4471.

Data Availability Statement

The data that supports the findings of this study are available in the supplementary material of this article

References

1. Pashley DH. Dynamics of the pulpo-dentin complex. Crit Rev Oral Biol Med. 1996;7(2):104-133.
2. Cho YS, Ryu CH, Won JH, et al. Rat odontoblasts may use glutamate to signal dentin injury. Neuroscience. 2016;29(335):54-63.
3. Lee Y-L, Liu J, Clarkson BH, Lin C-P, Godovikova V, Ritchie HH. Dentin-pulp complex responses to carious lesions. Caries Res. 2006;40(3):256-264.
4. Lin M, Luo ZY, Bai BF, Xu F, Lu TJ. Fluid mechanics in dentinal microtubules provides mechanistic insights into the difference between hot and cold dental pain. PLOS One. 2011;6(3):e18068.
5. Veerayutthwilai O, Byers MR, Pham T-TT, Darveau RP, Dale BA. Differential regulation of immune responses by odontoblasts. Oral Microbiol Immunol. 2007;22(1):5-13.
6. Won J, Vang H, Kim JH, Lee PR, Kang Y, Oh SB. TRPM7 mediates mechanosensitivity in adult rat odontoblasts. J Dent Res. 2018;97(9):1039-1046.
7. Arana-Chavez VE, Massa LF. Odontoblasts: the cells forming and maintaining dentine. Int J Biochem Cell Biol. 2004;36(8):1367-1373.
8. Balic A, Thesleff I. Chapter seven—tissue interactions regulating tooth development and renewal. Curr Top Dev Biol. 2015;115:157-186.
9. Thesleff I, Sharpe P. Signalling networks regulating dental development. Mech Dev. 1997;67(2):111-123.
10. Bae C-H, Kim T-H, Chu J-Y, Cho E-S. New population of odontoblasts responsible for tooth root formation. Gene Expr Patterns. 2013;13(5):197-202.
11. Xiong J, Gronthos S, Bartold PM. Role of the epithelial cell rests of Malassez in the development, maintenance and regeneration of periodontal ligament tissues. Periodontol. 2000;63:217-233.
12. Yamashiro T, Zheng L, Shitaku Y, et al. Wnt10a regulates dentin sialophosphoprotein mRNA expression and possibly links odontoblast differentiation and tooth morphogenesis. Differentiation. 2007;75(5):452-462.
13. Krivanek J, Adameyko I, Fried K. Heterogeneity and developmental connections between cell types inhabiting teeth. Front Physiol. 2017;8:376.
14. Khatibi Shahidi M, Krivanek J, Kaukua N, et al. Three-dimensional imaging reveals new compartments and structural adaptations in odontoblasts. J Dent Res. 2015;94(7):945-954.
15. Smith AJ, Cassidy N, Perry H, Begue-Kirn C, Ruch J-V, Lesot H. Reactionary dentinogenesis. Int J Dev Biol. 1995;39(1):273-280.
16. Smith AJ, Scheven BA, Takahashi Y, Ferracane JL, Shelton RM, Cooper PR. Dentine as a bioactive extracellular matrix. Arch Oral Biol. 2012;57(2):109-121.
17. Couve E, Osorio R, Schmachtenberg O. The amazing odontoblast: activity, autophagy, and aging. J Dent Res. 2013;92(9):765-772.
18. Beertsen W, Niehof A. Root-analogue versus crown-analogue dentin: a radioautographic and ultrastructural investigation of the mouse incisor. Anat Rec. 1986;215(2):106-118.
19. Steinfort J, van den Bos T, Beertsen W. Differences between enamel-related and cementum-related dentin in the rat incisor with special emphasis on the phosphoproteins. J Biol Chem. 1989;264(5):2840-2845.
20. Simon S, Smith AJ, Lumley PJ, et al. Molecular characterization of young and mature odontoblasts. Bone. 2009;45(4):693-703.
21. Sun Y, Gandhi V, Prasad M, et al. Distribution of small integrin-binding ligand, N-linked glycoproteins (SIBLING) in the condylar cartilage of rat mandible. Int J Oral Maxillofac Surg. 2010;39(3):272-281.
22. Toyosawa S, Okabayashi K, Komori T, Ijuhin N. mRNA expression and protein localization of dentin matrix protein 1 during dental root formation. Bone. 2004;34(1):124-133.
23. Vijaykumar A, Ghassem-Zadeh S, Vidovic-Zdrilic I, et al. Generation and characterization of DSPP-cerulean/DMP1-cherry reporter mice. Genesis. 2019;57:e23324.
24. Boran T, Peterkova R, Lesot H, Lyons DB, Peterka M, Klein OD. Temporal analysis of ectopic enamel production in incisors from sprouty mutant mice. J Exp Zoolog B Mol Dev Evol. 2009;312B(5):473-485.
25. Klein OD, Lyons DB, Balooch G, et al. An FGF signaling loop sustains the generation of differentiated progeny from stem cells in mouse incisors. Development. 2008;135(2):377-385.
26. Klein OD, Minowada G, Peterkova R, et al. Sprouty genes control diastema tooth development via bidirectional antagonism of epithelial-mesenchymal FGF signaling. Dev Cell. 2006;11(2):181-190.
27. Shim K, Minowada G, Coling DE, Martin GR. Sprouty2, a mouse deafness gene, regulates cell fate decisions in the auditory sensory epithelium by antagonizing FGF signaling. Dev Cell. 2005;8(4):553-564.
28. Krivanek J, Soldatov RA, Kastriti ME, et al. Dental cell type atlas reveals stem and differentiated cell types in mouse and human teeth. Nat Commun. 2020;11(1):4816.
29. Schneider CA, Rasband WS, Eliceiri KW. NIH Image to ImageJ: 25 years of image analysis. Nature Methods. 2012;9(7):671-675. https://doi.org/10.1038/nmeth.2089
30. An Z, Sabalic M, Bloomquist RF, Fowler TE, Streelman T, Sharpe PT. A quiescent cell population replenishes mesenchymal stem cells to drive accelerated growth in mouse incisors. Nat Commun. 2018;9(1):1-9.
31. Harada H, Kettunen P, Jung H-S, Mustonen T, Wang YA, Thesleff I. Localization of putative stem cells in dental epithelium and their association with notch and Fgf signaling. J Cell Biol. 1999;147(1):105-120.
32. Bleckert A, Photowala H, Alford S. Dual pools of actin at presynaptic terminals. J Neurophysiol. 2012;107(12):3479-3492.
33. Limbeck A, Brunnbauer L, Lohninger H, et al. Methodology and applications of elemental mapping by laser induced breakdown spectroscopy. Anal Chim Acta. 2021;22(1147):72-98.
34. Modlitbová P, Pořízka P, Kaiser J. Laser-induced breakdown spectroscopy as a promising tool in the elemental bioimaging of plant tissues. TrAC Trends in Analytical Chemistry, 2020;122:115729. https://doi.org/10.1016/j.trac.2019.115729
35. Pořízka P, Klus J, Képeš E, Prochazka D, Hahn DW, Kaiser J. On the utilization of principal component analysis in laser-induced breakdown spectroscopy data analysis, a review. Spectrochim Acta Part B Atomic

Spectroscopy. 2018;148:65-82. https://doi.org/10.1016/j.sab.2018.05.030

36. Li C, Jing Y, Wang K, et al. Dentinal mineralization is not limited in the mineralization front but occurs along with the entire odontoblast process. Int J Biol Sci. 2018;14(7):693-704.
37. Mishima H, Kozawa Y, Sakae T. Two patterns of calcification in rat and rabbit incisor dentin. In Suga S, Nakahara H, eds. Mechanisms and phylogeny of mineralization in biological systems. Tokyo: Springer Japan; 1991 pp 223-227.
38. Shuhaibar N, Hand AR, Terasaki M. Odontoblast processes of the mouse incisor are plates oriented in the direction of growth. Anat Rec. 2020;304(8):1820-1827.
39. Foster BL, Soenjaya Y, Nociti FH, et al. Deficiency in acellular cementum and periodontal attachment in Bsp null mice. J Dent Res. 2013;92(2):166-172.
40. Imhof T, Balic A, Heilig J, et al. Pivotal role of tenascin-W (-N) in postnatal incisor growth and periodontal ligament remodeling. Front Immunol. 2021;11:608223.
41. Tummers M, Thesleff I. Observations on continuously growing roots of the sloth and the K14-Eda transgenic mice indicate that epithelial stem cells can give rise to both the ameloblast and root epithelium cell lineage creating distinct tooth patterns. Evol Dev. 2008;10(2):187-195.
42. Wen Q, Jing J, Han X, et al. Runx2 regulates mouse tooth root development via activation of WNT inhibitor NOTUM. J Bone Miner Res. 2020;35(11):2252-2264.
43. Lin Y, Xiao Y, Lin C, et al. SALL1 regulates commitment of odontoblast lineages by interacting with RUNX2 to remodel open chromatin regions. Stem Cells. 2021;39(2):196-209.
44. Huang X, Xu X, Bringas P, Hung YP, Chai Y. Smad4-Shh-Nfic Signaling Cascade-Mediated Epithelial-Mesenchymal Interaction is Crucial in Regulating Tooth Root Development. J Bone Miner Res. 2010;25(5):1167-1178. https://doi.org/10.1359/jbmr.091103
45. Kim T-H, Bae C-H, Yang S, Park J-C, Cho ES. Nfic regulates tooth root patterning and growth. Anat Cell Biol. 2015;48(3):188-194.
46. Liu Y, Feng J, Li J, Zhao H, Ho T-V, Chai Y. An Nfic-hedgehog signaling cascade regulates tooth root development. Development. 2015;142(19):3374-3382.
47. Steinfort J, Deblauwe BM, Beertsen W. The inorganic components of cementum- and enamel-related dentin in the rat incisor. J Dent Res. 1990;69(6):1287-1292.
48. Gradl R, Zanette I, Ruiz-Yaniz M, et al. Mass density measurement of mineralized tissue with grating-based X-ray phase tomography. PLOS One. 2016;11(12):e0167797.
49. Manly RS, Hodge HC, Ange LE. Density and refractive index studies of dental hard tissues: II. Density distribution curves 1,2. J Dent Res. 1939;18(3):203-211.